Phonon amplification in two coupled cavities containing one mechanical resonator

Hui Wang,[1,2] Zhixin Wang,[2] Jing Zhang,[3,4] Şahin Kaya Özdemir,[5] Lan Yang,[5] and Yu-xi Liu[1,2,4,*]

[1]*Institute of Microelectronics, Tsinghua University, Beijing 100084, China*

[2]*Department of Microelectronics and Nanoelectronics, Tsinghua University, Beijing 100084, China*

[3]*Department of Automation, Tsinghua University, Beijing 100084, China*

[4]*Tsinghua National Laboratory for Information Science and Technology (TNList), Beijing 100084, China*

[5]*Department of Electrical and Systems Engineering, Washington University, St. Louis, Missouri 63130, USA*

(Received 22 May 2014; published 7 November 2014)

We study a general theory of phonon lasing [I. S. Grudinin *et al.*, Phys. Rev. Lett. **104**, 083901 (2010)] in coupled optomechancial systems. We derive the dynamical equation of the phonon lasing using supermodes formed by two cavity modes. A general threshold condition for phonon lasing is obtained. We also show the differences between phonon lasing and photon lasing, generated by photonic supermodes and a two-level atomic ensemble, respectively. We find that the phonon lasing can be produced in a certain parameter regime near the threshold. The phase diagrams and degrees of second-order coherence for the phonon lasing are also studied to show some interesting phenomena that cannot be observed in the photon lasing generated by two-level atomic ensembles.

DOI: 10.1103/PhysRevA.90.053814 PACS number(s): 42.50.Pq, 42.50.Dv, 42.50.Ct, 71.36.+c

I. INTRODUCTION

Phonons are quanta of sound and are a very important concept in condensed matter physics. They exist as vibrating modes in various physical systems, including single trapped ions [1], atoms in solid-state materials [2], and macroscopic mechanical resonators [3]. Phonons are very similar to photons in the sense that both are bosonic particles and obey Bose-Einstein statistics. Thus, the phenomena occurring in photons are quite often brought to phonons. For instance, in analog to coherent and squeezed photon states, squeezed phonon states [4] have been proposed to be generated in bulk solid-state materials by using second-order Raman scattering and explored to modulate quantum fluctuations of atomic displacements. The coherent phonon generation via impulsive stimulated Raman scattering in the condensed media [5] and the phonon stimulated emission have also been studied [6–9].

Reaching the quantum mechanical regime for vibrating modes of macroscopic mechanical resonators is a long-standing goal [3]. Both mechanical resonators and single-mode cavity fields can be modeled as harmonic oscillators. The quanta corresponding to quantized cavity fields and mechanical modes are called photons and phonons, respectively. Thus, it is reasonable to expect that mechanical resonators can play the role of single-mode cavity fields in quantum optics, and help to realize mechanical quantum electrodynamics (QED) by replacing the single-mode cavity field with a mechanical resonator in its quantum regime. Experimentalists have shown that the usual Jaynes-Cumming model in the cavity QED can be realized by coupling a superconducting qubit to a mechanical resonator [10–12]. Recently, the single-mode phonon cavity has also been experimentally demonstrated [13]. Moreover, several methods have been developed in optomechanical systems for cooling mechanical resonators with low frequencies to their quantum ground states by coupling them to a single-mode microwave or optical field via the radiation pressure [14]. In particular, the nonclassical phonon states, including the single-phonon state and entangled phonon states, can be engineered [15,16] by virtue of the optomechanical coupling between mechanical resonators and a cavity field when the single-photon blockade occurs in the optomechanical system. These achievements lay a solid foundation to manipulate phonon states at the single-photon level in optomechanical systems [17,18].

It is well known that photon lasing can be generated when the stimulated emission of photons is coherently amplified by a gain medium inside a cavity. Similarly, several theoretical proposals were put forward to generate phonon lasing via coherent amplification of stimulated emission of phonons in various physical systems, e.g., the quantum dot [19–21], ultracold atomic gas [22], nanomagnets [23], acoustical cavities [24], and double-barrier systems [25]. The amplification of mechanical oscillations was also theoretically studied by coupling a nanomechanical resonator to polarized paramagnetic nuclei [26]. Such so-called phonon lasing was experimentally demonstrated in the systems of vibrating microscopic particles (e.g.,trapped magnesium ions [27]), electromechanical resonators [28], and superlattice structures [29]. Recently reported experiments on phonon lasing in optomechanical systems [30,31] and also in an optomechanical system coupled to a cavity [32] are of particular interest, and have been a focus of attention.

In the experiment reported in Ref. [32], two degenerate microtoroid whispering gallery mode optical resonators (that is, they have the same resonance frequency) are coupled in a controllable way through their evanescent fields. One of the cavities is coupled to a mechanical resonator via the radiation pressure, and thus the optomechanical system is formed. The coupling between the two cavity modes lifts their degeneracy and leads to two normal supermodes, which are symmetric and antisymmetric combinations of the two degenerate cavity modes [32]. The frequency difference between the two supermodes is proportional to the coupling strength between the two degenerate cavity modes and can be tuned to resonantly interact with the mechanical mode. Using such

*yuxiliu@mail.tsinghua.edu.cn

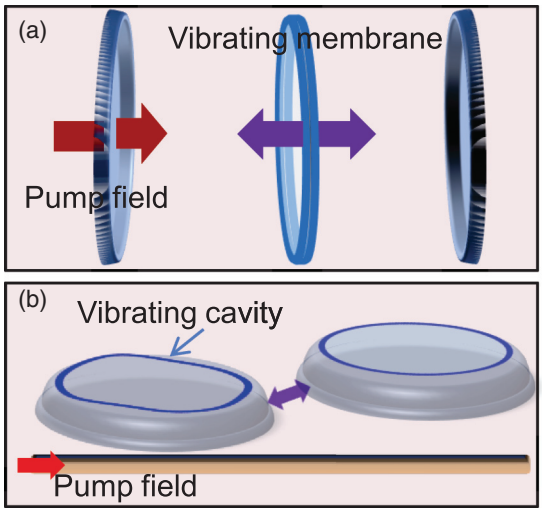

FIG. 1. (Color online) (a) A movable mirror is placed inside a cavity, and is coupled to the left modes a_L and right a_R of the cavity. (b) A cavity is coupled to an optomechanical system. In both cases, we assume that the two cavity fields have the same frequencies and decay rates. A classical driving field is assumed to be applied to the left cavity.

an interaction, the phonon lasing can be generated [32]. This ingenious design is very similar to a laser system composed of a two-level atomic ensemble interacting with single-mode cavity fields [33,34]. Although the threshold condition on the phonon lasing in the coupled cavity system has been discussed in Ref. [32], the stability of the system, lasing phonon statistics, and threshold still need to be rigorously analyzed. Motivated by the experiment on phonon lasing [32] and considering both the theoretical [35–41] and the experimental [42,43] studies on coupled optomechanical systems from optical to microwave frequencies [14,44], we have analyzed the phonon lasing in coupled optomechanical systems by using a completely quantum theoretical approach.

Our paper is organized as follows. In Sec. II, we give the Hamiltonian which is used to describe two possible experimental setups for phonon generation, and then obtain the supermode description for the phonon lasing. In Sec. III, we derive the steady-state solution using the equations of motion for the variables of the cavity fields and the mechanical resonator. In particular, we study how the phonon number changes with the driving field. We also show how the stability of the system varies with the driving field. In Sec. IV, we derive the equation of phonon lasing and analyze the relation between the mechanical gain and population inversion. We also carefully study the phase diagram of the phonon lasing by using equations of motion in the phonon-stimulated regime. In Sec. V, the phonon statistics is studied. Finally, we summarize and discuss our results.

II. THEORETICAL MODEL

As schematically shown in Fig. 1(a) and Fig. 1(b), we study two very similar systems, which contain two cavities and a mechanical resonator. Hereafter, we call the two cavities the left and the right cavities, respectively. These two cavities are coupled to each other with the coupling strength g. The annihilation (creation) operators for the left and the right cavity fields are defined as a_L ($a_L^\dagger$) and a_R ($a_R^\dagger$). We assume that a classical driving field (i.e., pump field) with the frequency ω_d is applied to the left cavity with the coupling strength Ω, which is proportional to the intensity of the driving field. Therefore, we call the parameter Ω either the driving strength or the coupling strength. We use χ to represent the coupling strength between the cavity field and the mechanical resonator via the radiation pressure. We also assume that the optical modes (one from each cavity) are frequency-degenerate (i.e., they have the same frequency) when the cavities are solitary, that is, when they are decoupled.

The difference between the two systems shown in Fig. 1(a) and Fig. 1(b) is as follows. In the system shown in Fig. 1(a), both the left and the right cavity fields interact with the mechanical resonator, whereas in the system shown in Fig. 1(b) only the right cavity field is coupled to the mechanical resonator. We assume that the one, shown in Fig. 1(a), contains a vibrating dielectric membrane (e.g., in Ref. [45]), which is placed the midway between the two mirrors. Then the corresponding Hamiltonian of the system is given as [35–38]

$$\begin{aligned} H_0 &= \hbar\omega_c a_L^\dagger a_L + \hbar\omega_c a_R^\dagger a_R + \hbar g(a_L^\dagger a_R + a_R^\dagger a_L) \\ &\quad + \hbar\omega_m b^\dagger b - \hbar\chi(a_L^\dagger a_L - a_R^\dagger a_R)(b^\dagger + b) \\ &\quad + i\hbar[\Omega\exp(-i\omega_d t)a_L^\dagger - \text{H.c.}]. \end{aligned} \tag{1}$$

We assume that the other one, shown in Fig. 1(b), consists of a cavity, which is coupled to an optomechanical system (e.g., in Ref. [32]). The Hamiltonian of this system is described [39–41] as

$$\begin{aligned} \widetilde{H} &= \hbar\omega_c a_L^\dagger a_L + \hbar\omega_c a_R^\dagger a_R + \hbar g(a_L^\dagger a_R + a_R^\dagger a_L) \\ &\quad + \hbar\omega_m b^\dagger b - \hbar\chi a_L^\dagger a_L(b^\dagger + b) \\ &\quad + i\hbar[\Omega\exp(-i\omega_d t)a_L^\dagger - \text{H.c.}]. \end{aligned} \tag{2}$$

Here, we note that the parameter ω_m in both Eq. (1) and Eq. (2) represents the frequency of the mechanical resonator. b and $b^\dagger$ denote the annihilation and creation operators of the mechanical mode with the frequency ω_m.

Using the supermode operators $a_1 = (a_L + a_R)/\sqrt{2}$ and $a_2 = (a_L - a_R)/\sqrt{2}$ as defined in Ref. [32], and assuming that the frequency ω_m of the mechanical resonator is resonant or near resonant with the energy gap $2g$ between the two supermodes, we can rewrite the Hamiltonian H_0 in Eq. (1) as

$$\begin{aligned} H_0 &= \hbar\omega_m b^\dagger b - \hbar\chi(a_1^\dagger a_2 b + a_2^\dagger a_1 b^\dagger) + \hbar(g-\Delta)a_1^\dagger a_1 \\ &\quad - \hbar(g+\Delta)a_2^\dagger a_2 + \frac{i\hbar}{\sqrt{2}}[\Omega(a_1^\dagger + a_2^\dagger) - \text{H.c.}], \end{aligned} \tag{3}$$

in the basis of the supermodes by neglecting antirotating terms $a_1^\dagger a_2 b^\dagger$ and $a_1 a_2^\dagger b$. Here, the parameters $g-\Delta$ and $g+\Delta$ denote the frequencies of the supermodes 1 and 2, respectively. $\Delta = \omega_d - \omega_c$ is the detuning between the driving field and cavity mode. It is easy to to show that if χ in Eq. (3) is changed into $-\chi/2$, then we obtain the supermode representation for the system shown in Fig. 1(b) with the Hamiltonian in Eq. (2). Thus, we will only deal with the Hamiltonian H_0 in Eq. (3) corresponding to Fig. 1(a) in the following calculations. All

discussions related to the Hamiltonian H_0 can be generalized to that $\widetilde{H}$ in Eq. (2).

Using the Hamiltonian in Eq. (3) and considering the environmental effects, we can write the equations of motion for the cavity and mechanical modes of the system as follows:

$$\frac{da_1}{dt} = -\left[\frac{\gamma_c}{2} + i(g-\Delta)\right]a_1 + i\chi a_2 b + \frac{\Omega}{\sqrt{2}} + \Gamma_1(t), \tag{4}$$

$$\frac{da_2}{dt} = -\left[\frac{\gamma_c}{2} - i(g+\Delta)\right]a_2 + i\chi a_1 b^\dagger + \frac{\Omega}{\sqrt{2}} + \Gamma_2(t), \tag{5}$$

$$\frac{db}{dt} = -(\gamma_m + i\omega_m)b + i\chi a_2^\dagger a_1 + \sqrt{2\gamma_m}b_{\rm in}(t). \tag{6}$$

Here, we assume that decay rates γ_L and γ_R of the left and right cavities are the same, i.e., $\gamma_L \equiv \gamma_R = \gamma_c$, and the decay rate of the mechanical resonator is assumed as γ_m. $\Gamma_1(t)$, $\Gamma_2(t)$, and $b_{\rm in}(t)$ represent fluctuation operators corresponding to the supermodes and the mechanical resonator. As discussed in Appendix A, the correlation functions of the fluctuation operators of the supermodes in the time domain under the Markovian approximation are given as

$$\langle\Gamma_1(t)\Gamma_1^\dagger(t')\rangle = \langle\Gamma_2(t)\Gamma_2^\dagger(t')\rangle = \gamma_c\delta(t-t'), \tag{7}$$

$$\langle\Gamma_1^\dagger(t)\Gamma_1(t')\rangle = \langle\Gamma_2^\dagger(t)\Gamma_2(t')\rangle = 0. \tag{8}$$

Here, we assume that the thermal energy due to environmental temperature T is sufficiently lower than the transition energies of the cavity modes; thus the effect of the environmental temperature on the cavity modes is negligibly small. This assumption might not be valid in the representation of the supermodes; however, for the sake of simplicity, we here neglect the temperature effect on the transition between the two supermodes, and only consider the temperature effect on the mechanical resonator. Then, the correlation functions of the fluctuation operators of the mechanical resonator become

$$\langle b_{\rm in}^\dagger(t)b_{\rm in}(t')\rangle = n_b(T)\delta(t-t'), \tag{9}$$

$$\langle b_{\rm in}(t')b_{\rm in}^\dagger(t)\rangle = [n_b(T)+1]\delta(t-t'), \tag{10}$$

where $n_b(T) = 1/[\exp(\hbar\omega_m/K_BT) - 1]$ denotes the thermal phonon number of the mechanical resonator, and K_B is the Boltzmann constant.

III. STEADY-STATES ANALYSIS

Let us now study the steady state of the coupled optomechanical systems. First, we show that the bistable behavior can be observed in these coupled systems even in the blue detuning regime. We find that there exists unconventional bistable behavior in the limit of a very strong driving field. We also analyze the stability under small disturbances in the parameter regime of the coherent phonon amplification.

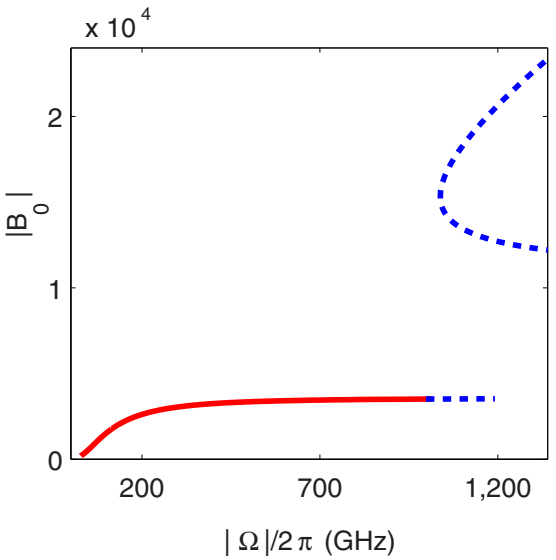

FIG. 2. (Color online) The steady-state value $|B_0|$ of the mechanical mode is plotted as a function of the coupling strength $|\Omega|/(2\pi)$ between the classical driving field and the cavity field. Other parameters are assumed as $\omega_m/(2\pi) = 23.4$ MHz, $\chi/(2\pi) = 1570$ Hz, $\gamma_m/(2\pi) = 0.125$ MHz, $\gamma_c/(2\pi) = 4.8$ MHz, $g/(2\pi) = 11.7$ MHz $= \omega_m/2$, and $\Delta = g/2$.

A. Mechanical bistability

Using the semiclassical and mean-field approximations, e.g., $\langle a_2 b\rangle = \langle a_2\rangle\langle b\rangle$, from Eqs. (4)–(6), we can obtain equations of motion for the average values of the system variables a_i $(i = 1,2)$ and b as

$$\langle\dot{a}_1\rangle = -\left[\frac{\gamma_c}{2} + i(g-\Delta)\right]\langle a_1\rangle + i\chi\langle a_2\rangle\langle b\rangle + \frac{\Omega}{\sqrt{2}}, \tag{11}$$

$$\langle\dot{a}_2\rangle = -\left[\frac{\gamma_c}{2} - i(g+\Delta)\right]\langle a_2\rangle + i\chi\langle a_1\rangle\langle b^\dagger\rangle + \frac{\Omega}{\sqrt{2}}, \tag{12}$$

$$\langle\dot{b}\rangle = -\gamma_m\langle b\rangle - i\omega_m\langle b\rangle + i\chi\langle a_2^\dagger\rangle\langle a_1\rangle. \tag{13}$$

If we define the steady-state values of the cavity and the mechanical modes as $\langle a_1\rangle_s = A_1$, $\langle a_2\rangle_s = A_2$, and $\langle b\rangle_s = B_0$, respectively, and set $\langle\dot{a}_1\rangle_s = \langle\dot{a}_2\rangle_s = \langle\dot{b}\rangle_s = 0$, then we can find that the driving strength Ω and the mechanical mode B_0 satisfy the following equation:

$$|\Omega|^2 = \frac{2B_0(\gamma_m + i\omega_m)\left[(|\xi|^2 - \Delta^2 + \chi^2|B_0|^2)^2 + \gamma_c^2\Delta^2\right]}{i\chi[\xi^2 + (\chi B_0 - \Delta)^2]}, \tag{14}$$

with $\xi = \gamma_c/2 - ig$. To make the equality sign in Eq. (14) valid, the imaginary part of the right-hand side of Eq. (14) has to be zero. This results in a constraint for the phonon lasing. Using Eq. (14) and also considering the above mentioned constraint, we plot $|B_0|$ as a function of the coupling strength $|\Omega|$ in Fig. 2, where the red solid curve represents the stable region of the phonon mode, while the blue dashed curve represents the boundary between stable and unstable regions. When the coupling strength Ω is increased to a critical point, the system becomes unstable and the bistable behaviors of the phonon mode are observed. In contrast to single-mode

optomechanical systems where the bistability occurs only in the red-detuning regime [46], the bistability of the coupled optomechanical systems can be observed in the blue-detuning regime $\omega_d > \omega_c$.

From Fig. 2, we also find that the curve of the steady-state value $|B_0|$ of the phonon mode versus the coupling strength Ω does not have the usual S shape. This unconventional bistable phenomenon has recently been studied in a hybrid optomechanical system where the cavity mode was strongly coupled to the excitons in a quantum well [47]. The coupling between photons and phonons in an optomechanical system can be simultaneously both dispersive and dissipative. The dispersive coupling is described by $a_i^\dagger a_i(b^\dagger + b)$ as in Eq. (1), where $i = R, L$. The dissipative coupling between photons and phonons usually results from the variation of the damping rate [48] of the cavity field induced by the mechanical resonator or the driving field, and is described by $(a_i^\dagger + a_i)(b^\dagger + b)$, which can be obtained with a displacement of the cavity field in Eq. (1) under the strong driving condition. This dissipative coupling together with the dispersive coupling results in the unconventional bistable phenomenon in the optomechanical systems [47]. The bistability of the photon mode in optomechanical systems is usually found in the regime where the dispersive coupling term is predominant. The strong Kerr nonlinearity and negligibly small dissipative coupling, then lead to the common S-shaped bistability curves for both the cavity field and the mechanical resonator. If both the coupling between two cavity modes and the driving field are very strong, then the dissipative coupling term will also contribute, leading to the unconventional bistability quantified by the branching observed in Fig. 2. The red-solid curve in Fig. 2 denotes the stable regime whereas the blue-dashed curve describes the unstable regime.

B. Stabilities

To discuss the stability of the system against small perturbations, let us now express the variables a_1, a_2, and b as the sums of their stable steady-state values and small fluctuation operators, that is,

$$a_1(t) = A_1 + \Lambda_1(t), \tag{15}$$

$$a_2(t) = A_2 + \Lambda_2(t), \tag{16}$$

$$b(t) = B_0 + \beta(t). \tag{17}$$

The expressions of $a_1^\dagger(t)$, $a_2^\dagger(t)$, and $b^\dagger(t)$ are obtained by taking the Hermitian conjugates of $a_1(t)$, $a_2(t)$, and $b(t)$, respectively. Here, the average values of fluctuation terms are assumed to be zero; i.e., $\langle\Lambda_1^\dagger(t)\rangle = \langle\Lambda_2^\dagger(t)\rangle = \langle\beta(t)\rangle = 0$. The steady-state values A_1, A_2, B_0 and their complex conjugates can be easily obtained from Eqs. (11)–(13) by setting all time derivatives to zero. Then we can write the linearized dynamical equations of the fluctuation operators up to their first orders as

$$\frac{d}{dt}\vec{u} = M\vec{u}. \tag{18}$$

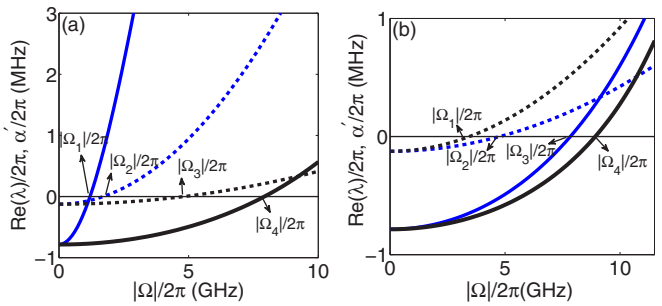

FIG. 3. (Color online) The real part of the eigenvalues Re(λ) of the matrix M in Eq. (19) and the net gain α' in Eq. (31) of phonons versus the coupling strength $|\Omega|$. Solid curves describe Re(λ), and the dashed curves correspond to α'. (a) For different detunings Δ, e.g., blue curves correspond to $\Delta = g$, while the black curves correspond to $\Delta = g/2$. We set $\gamma_c/(2\pi) = 4.8$ MHz. The points $|\Omega_1|/(2\pi)$ and $|\Omega_4|/(2\pi)$ correspond to Re(λ) = 0; however $|\Omega_2|/(2\pi)$ and $|\Omega_3|/(2\pi)$ correspond to $\alpha' = 0$. (b) For different decay rates, e.g., the blue curves correspond to $\gamma_c/(2\pi) = 4.8$ MHz, while the black curves correspond to $\gamma_c/(2\pi) = 2.8$ MHz. Here, we set $\Delta = g/2$. The points $|\Omega_3|/(2\pi)$ and $|\Omega_4|/(2\pi)$ correspond to Re(λ) = 0, whereas $|\Omega_1|/(2\pi)$ and $|\Omega_2|/(2\pi)$ correspond to $\alpha' = 0$. The other parameters are the same as in Fig. 2 except the coupling strength g between two cavities; its value can be obtained from the quantity $\delta/(2\pi) = (2g - \omega_m)/(2\pi) = 1$ MHz.

Here, the matrix M is given as

$$M = i\chi \begin{pmatrix} \frac{\epsilon_1}{i\chi} & 0 & B_0 & 0 & A_2 & 0 \\ 0 & \frac{\epsilon_1^*}{i\chi} & 0 & -B_0^* & 0 & -A_2^* \\ B_0^* & 0 & \frac{\epsilon_2}{i\chi} & 0 & 0 & A_1 \\ 0 & -B_0 & 0 & \frac{\epsilon_2^*}{i\chi} & -A_1^* & 0 \\ A_2^* & 0 & 0 & A_1 & \frac{\epsilon_3}{i\chi} & 0 \\ 0 & -A_2 & -A_1^* & 0 & 0 & \frac{\epsilon_3^*}{i\chi} \end{pmatrix}, \tag{19}$$

where $\epsilon_1 = -(\gamma_c/2) - i(g - \Delta)$, $\epsilon_2 = -(\gamma_c/2) + i(g + \Delta)$, and $\epsilon_3 = -\gamma_m - i\omega_m$. The vector $\vec{u}$ in Eq. (18) is defined as $\vec{u} = (\Lambda_1\ \Lambda_1^\dagger\ \Lambda_2\ \Lambda_2^\dagger\ \beta\ \beta^\dagger)^T$, where the superscript T denotes the transpose.

The stability of the system is determined by the eigenvalues of the matrix M. If the real parts of the eigenvalues of M are all negative, then the system is stable. Otherwise the system is unstable. It is not easy to analytically obtain the eigenvalues of M. However, we can numerically calculate them. The matrix M includes three pairs of conjugate eigenvalues. We numerically find that the real parts of two pairs of the eigenvalues are always negative near the threshold; thus we need only to calculate the real part Re(λ) of the eigenvalues for the remaining pair. In Fig. 3, the real parts Re(λ) of these two eigenvalues are plotted as a function of the coupling strength $|\Omega|$. From Fig. 3(a), we find that the system has a larger stable region for the case $\Delta = g/2$ than the case $\Delta = g$. Figure 3(b) shows that the stable region of the system becomes smaller for faster decay rates of the cavity field. To show the stability of the phonon lasing, the net gain α' of the phonon lasing is also plotted as a function of the coupling strength $|\Omega|$ in Fig. 3. The

detailed discussions about the relation between the gain of the phonon lasing and the stability will be given when Eq. (31) is introduced.

IV. PHONON LASING

Let us now discuss several aspects of phonon lasing. Under the adiabatic approximation for the variables of supermodes, we derive the dynamical equation of the phonon mode and revisit the threshold condition for phonon lasing which was obtained in Ref. [32]. We discuss the relation between the gain and the population inversion of the two supermodes. We also define an effective potential for the phonon mode near the threshold in a special case, and discuss the phase diagram of phonon lasing.

A. Phonon lasing equation and threshold condition

To find the relation between the phonon lasing and the population inversion of the supermodes, and also to compare the phonon lasing with the photon lasing generated by two-level atomic ensemble, we define the ladder and population inversion operators via the angular momentum operators constructed by two bosonic supermode operators [49]. Because the energy of the supermode 1 is larger than that of the supermode 2, we define the angular momentum operators as $J_+ = a_1^\dagger a_2$, $J_- = a_2^\dagger a_1$, and $J_z = (a_1^\dagger a_1 - a_2^\dagger a_2)/2$, which describes the population difference between the supermode 1 and the supermode 2. Therefore, $J_\pm$ and J_z correspond to the ladder operators and the population inversion operator in the photon lasing using a two-level atomic ensemble [34].

Using Eqs. (4)–(6) and also their Hermitian conjugates, the dynamical equations for the variables J_- and J_z can be obtained as

$$\frac{dJ_-}{dt} = -\gamma_c J_- - 2ig J_- - 2i\chi J_z b + \frac{\Omega^*}{\sqrt{2}}a_1 + \frac{\Omega}{\sqrt{2}}a_2^\dagger + \Gamma_2^\dagger(t)a_1 + a_2^\dagger\Gamma_1(t), \tag{20}$$

$$\frac{dJ_z}{dt} = -\gamma_c J_z + i\chi J_+ b - i\chi J_- b^\dagger + \frac{\Omega}{2\sqrt{2}}a_1^\dagger + \frac{\Omega^*}{2\sqrt{2}}a_1 - \frac{\Omega}{2\sqrt{2}}a_2^\dagger - \frac{\Omega^*}{2\sqrt{2}}a_2 + \frac{1}{2}a_1^\dagger\Gamma_1(t) + \frac{1}{2}\Gamma_1^\dagger(t)a_1 - \frac{1}{2}a_2^\dagger\Gamma_2(t) - \frac{1}{2}\Gamma_2^\dagger(t)a_2, \tag{21}$$

$$\frac{db}{dt} = -\gamma_m b - i\omega_m b + i\chi J_- + \sqrt{2\gamma_m}b_{\rm in}(t). \tag{22}$$

The equation of motion in Eq. (22) for the phonon mode has the same form as that of the photon mode in the photon lasing generated by the two-level atomic ensemble [34]. However, we find that the equations of motion in Eqs. (20) and (21) for J_- and J_z are very different from those of the ladder and population inversion operators in the photon lasing generated by the two-level atomic ensemble [34].

In both Eq. (20) and Eq. (21), the parts, related to the ladder $J_\pm$ and population inversion J_z operators paired by two supermode operators, play the same role as those in the photon lasing generated by two-level atomic ensemble. These terms describe population transition processes between the supermode 1 and the supermode 2, which accompany the phonon emission and absorption. If the number of phonon emission is larger than the absorption, then it is possible to create coherent phonon amplification and realize phonon lasing in the coupled optomechanical system.

It is also easy to show that unpaired supermode operators, e.g., $(\Omega^* a_1 + \Omega a_2^\dagger)/\sqrt{2}$, also exist in Eqs. (20) and (21). These unpaired supermode operators are due to the classical driving field applied to the unpaired cavity field operator. Thus the driving part in the Hamiltonian, e.g., Eq. (1), cannot be expressed using paired angular momentum operators. This results in the mixing of the unpaired supermode operators and the angular momentum operators paired by the supermode operators in Eq. (20) and Eq. (21). This is the main difference between phonon lasing generated by supermodes here and photon lasing generated by two-level atomic ensemble [34]. Since these additional terms $(\Omega^* a_1 + \Omega a_2^\dagger)/\sqrt{2}$ and $[\Omega^*(a_1 - a_2) + \text{H.c.}]/2\sqrt{2}$ appear in Eq. (20) and Eq. (21), respectively, the phonon lasing studied here will show different behaviors compared to the photon lasing [34]. These terms might result in phonon lasing without population inversion between the two supermodes. However, the population inversion is a necessary condition for the photon lasing generated by the two-level atomic ensemble. These unpaired driving terms also result in new properties in the phase diagram of phonon lasing, which will be discussed below.

We assume that the decay rate γ_c of the cavity field is much larger than the decay rate γ_m of the mechanical resonator; then the variables J_- and J_z of the cavity fields will be subject to the dynamics of the mechanical resonator under the conditions that $\partial J_-/(\gamma_c \partial t) \ll J_-$ and $\partial J_z/(\gamma_c \partial t) \ll J_z$, which leads to the so-called adiabatical approximation. By setting $\partial J_-/\partial t = 0$ and $\partial J_z/\partial t = 0$, from Eqs. (20) and (21), we obtain

$$J_- = \frac{1}{\gamma_c + i\delta}\left[-2i\chi J_z b + \frac{1}{\sqrt{2}}(\Omega^* a_1 + \Omega a_2^\dagger)\right] + \frac{1}{\gamma_c + i\delta}[\Gamma_2^\dagger(t)a_1 + a_2^\dagger\Gamma_1(t)], \tag{23}$$

$$J_z = \frac{i\chi}{\gamma_c}(J_+ b - b^\dagger J_-) + \frac{\Omega a_1^\dagger - \Omega a_2^\dagger + \text{H.c.}}{2\sqrt{2}\gamma_c} + \frac{a_1^\dagger\Gamma_1(t) - a_2^\dagger\Gamma_2(t) + \text{H.c.}}{2\gamma_c}. \tag{24}$$

Here, $\delta = 2g - \omega_m$ is the detuning between the frequency of the two-level system formed by supermodes and that of the mechanical resonator [see the oscillating term $i2gJ_-$ in Eq. (20) for the equation of motion of J_-].

Substituting the expression of J_- into the dynamical equation of b in Eq. (22), we have

$$\frac{db}{dt} = -i\omega_m b - \left[\gamma_m - 2\frac{\chi^2 J_z}{\gamma_c + i\delta}\right]b + \frac{\alpha}{\sqrt{2}}(\Omega^* a_1 + \Omega a_2^\dagger) + \alpha[\Gamma_2^\dagger(t)a_1 + a_2^\dagger\Gamma_1(t)] + \sqrt{2\gamma_m}b_{\rm in}(t), \tag{25}$$

with $\alpha = i\chi/(\gamma_c + i\delta)$. If we neglect the third term of the right-hand side in Eq. (25) related to the supermodes a_1 and

a_2, then we find the gain of the phonon lasing as

$$G' = \mathrm{Re}\left(\frac{2\chi^2 J_z}{\gamma_c + i\delta}\right) = \frac{2\chi^2\gamma_c J_z}{\gamma_c^2 + (2g-\omega_m)^2}, \tag{26}$$

which is proportional to the population inversion operator J_z of two supermodes. We note that this is just the gain of the phonon lasing given in Ref. [32]. And also this gain is similar to that of the photon lasing [34]. However, the gain is significantly modified when the third term of the right-hand side of Eq. (25) is taken into account.

To obtain more exact expression for the gain of the phonon lasing when the driven terms for the supermodes are included, let us further adiabatically eliminate a_1 and a_2 in Eq. (25) by setting $\partial a_i/\partial t = 0$ (with $i = 1,2$) in Eqs. (4) and (5). In this case, Eq. (25) is expressed as

$$\frac{db}{dt} = -\left[\gamma_m - \frac{2\chi^2 J_z}{\gamma_c + i\delta} + \frac{i\Delta\gamma_c\chi^2|\Omega|^2}{(\gamma_c + i\delta)\left(N^2 + \Delta^2\gamma_c^2\right)}\right] b - i\omega_m b + i\frac{\chi|\Omega|^2[N(\gamma_c - i2g) + 2\Delta^2\gamma_c]}{2(\gamma_c + i\delta)\left(N^2 + \Delta^2\gamma_c^2\right)} + \Gamma(t), \tag{27}$$

where the parameter N is defined as $N = \gamma_c^2/4 + g^2 - \Delta^2 + \chi^2 b^\dagger b$. The expression of the noise term $\Gamma(t)$ is given in Eq. (A9) of Appendix A. The phonon lasing is fully determined by Eq. (27). For the simplicity of discussions, we only discuss the phonon lasing near the threshold. In this case, the average phonon number $n = b^\dagger b$ is negligibly small and the third term of the right-hand side of Eq. (27) is independent of n. Thus, the phonon amplification only depends on the first term on the right-hand side of Eq. (27). The imaginary part of the first term on the right-hand side of Eq. (27) denotes the frequency shift of the mechanical mode due to the coupling to the cavity fields, while the real part, depending on the plus or minus sign, describes the cooling or amplification of the mechanical mode. That is, when the real part of the first term on the right-hand side of Eq. (27) is larger than zero, the phonon mode can be amplified, and then the phonon lasing can be produced. Because γ_m describes the decay of the phonon lasing, the gain can only be derived from the second and the third terms within the bracket of the first term on the right-hand side of Eq. (27).

In the case in which the phonon number is negligibly small near the threshold, the gain G of the phonon lasing from the first term of Eq. (27) can be approximated as

$$G = G' - G'' \tag{28}$$

with G' given by Eq. (26) and

$$G'' = \frac{\Delta\delta\gamma_c\chi^2|\Omega|^2}{\left(\gamma_c^2 + \delta^2\right)\left(N^2 + \Delta^2\gamma_c^2\right)}, \tag{29}$$

which originates from the driving terms for the unpaired supermode operators in Eq. (20) and Eq. (21). It is clear that the gain is proportional to the population inversion J_z when $\Delta = \omega_d - \omega_c = 0$; therefore, the threshold condition in Ref. [32] is valid only when the cavity field is resonantly driven or $2g = \omega_m$. However, as shown in Eq. (28), the formula of the gain has an additional term when both $\omega_d \neq \omega_c$ and $\omega_m \neq 2g$. From Eq. (27), we can obtain the threshold condition $\gamma_m = G$; that is, the phonon mode can be amplified when $G > \gamma_m$. In particular, we find that the phonon mode can be amplified even if there is no population inversion, i.e., $\langle J_z\rangle = 0$ and then $G' = 0$, when both $\delta\Delta < 0$ and $\gamma_m + G'' < 0$.

B. Gain and population inversion of supermodes

As discussed above, for the photon lasing generated by the two-level atomic ensemble, the gain is proportional to the population inversion of the atomic ensemble. However, for the phonon lasing studied here in a coupled optomechanical system, Eq. (28) and Eq. (29) show that the gain is related not only to the population inversion of the supermodes, but also to the unpaired supermodes driven by the classical field when both Δ and δ are nonzero. The latter makes it possible to produce phonon lasing in the absence of population inversion. The phonon gain without population inversion is characterized by G'' in Eq. (29).

In Fig. 4, the total gain G and the gain G' due to the population inversion are plotted as a function of the coupling strength Ω and the detuning Δ for other given parameters. We have also plotted the gain $-G'' = G - G'$ in Fig. 4. We note that we have used the steady-state values of the cavity field and the mechanical mode for our numerical calculation, because the fluctuations are negligibly small for a strong driving field. Figure 4 shows that both $G > 0$ and $G' > 0$ increase with increasing the coupling strength Ω in the blue detuning regime with $\omega_d > \omega_c$ ($\Delta > 0$). However, in the red detuning regime $\omega_d < \omega_c$ ($\Delta < 0$), both $G < 0$ and $G' < 0$ decrease with increasing coupling strength Ω. We note that the peak and dip ridges in Fig. 4 correspond to the first-order

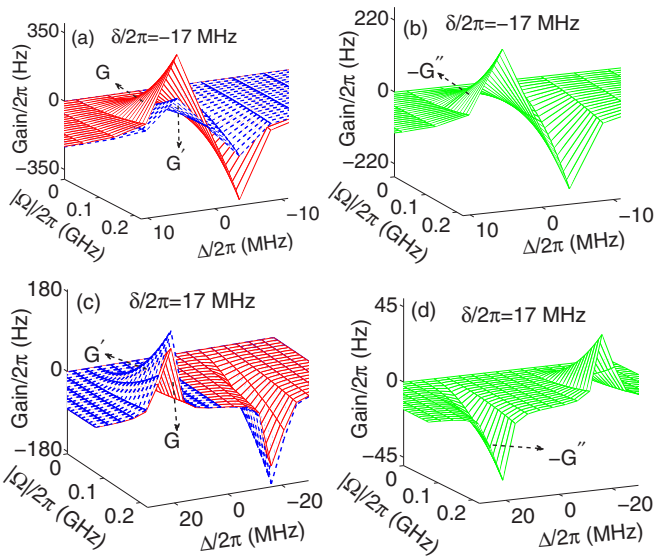

FIG. 4. (Color online) The gain of the mechanical mode as the function of the detuning Δ and the coupling strength Ω. In (a) and (c), the red and blue surfaces correspond to the total gain G and the gain G' resulted from the population inversion. The surfaces in (b) and (d) describe the gain $-G''$ which is from the classical driving to the supermodes. The coupling strength between two cavity modes can be obtained from $\delta/(2\pi) = -17$ MHz in (a) and (b) and 17 MHz in (c) and (d), the other parameter are same as in Fig. 2.

sideband excitation. The positions of resonant peaks in the ridge have been shifted compared to the usual optomechanical system. This results from the coupling between two cavity modes. The positions of resonant peaks can be tuned by the detuning $\delta = 2g - \omega_m$.

When the detuning δ is much smaller than the phonon frequency ω_m, the population inversion makes the main contributions to the phonon gain; that is, G' dominates. However, if the absolute value of δ is comparable with ω_m, the G'' has a significant effect on G in Eq. (28). Actually, as shown in Eq. (29), the sign of the production for Δ and δ determines the role of G''. In Figs. 4(a) and 4(b), $-G''$ has the same sign with G'; thus G is larger than G' in the blue detuning regime. However, if δ is changed to $\delta < 0$, then $-G''$ and G' have different signs, implying that the total G is smaller than G' as shown in Figs. 4(c) and 4(d). When the detuning Δ is large enough, the value of the gain approaches 0.

From Fig. 4, we can also find that both G and G' are positive in the blue detuning regime for the considered values of the parameters. This can be approximately verified using Eq. (11) and Eq. (12). The steady-state solutions of the two supermodes can be approximately obtained as $A_1 \approx \Omega/[\gamma_c/\sqrt{2} + i\sqrt{2}(g - \Delta)]$ and $A_2 \approx \Omega/[\gamma_c/\sqrt{2} - i\sqrt{2}(g + \Delta)]$ in the limit of weak radiation pressure and small phonon number near the threshold. In this case, we find that $|A_1|$ is always larger than $|A_2|$ in the blue detuning regime; thus the value of G' is positive in the blue detuning regime.

We conclude that both G', from the population inversion of supermodes, and $-G''$, from pure driving of the classical field to the supermodes, contribute to the phonon gain. However, they have different contributions in different parameter regimes. We note that even when the gain from the population inversion is zero, i.e., $G' = 0$, the gain of the phonon lasing is still different from that in the standard optomechanical system with the blue detuning driving field [50,51]. In Eq. (29), the linear coupling strength g of two cavity modes also affects the value of G'', but this parameter does not exist in the standard optomechanical system.

C. Phase diagram for phonon lasing near the threshold

Let us analyze the stabilization and phase transition of the phonon lasing near the threshold. To sketch the phase diagram of the phonon lasing, we further express J_z in Eq. (27) as the variables of mechanical mode by adiabatically eliminating the degrees of freedom for the cavity modes. As a result we express J_z as a function of the phonon operators in the regime close to the threshold such that $n = b^\dagger b \ll (\gamma_c^2 + \delta^2)/4\chi^2$ [see Eq. (B3) in Appendix B]. By replacing J_z in Eq. (25) with Eq. (B3), we obtain

$$\frac{db}{dt} = G_0 + G_1 b + G_2 b^\dagger b + G_3 bb - G_4 b^\dagger bb, \quad (30)$$

up to third-order terms of the operator b near the threshold of the phonon lasing. The coefficients G_i (for $i = 0,1,\ldots,4$) are found from Eqs. (B7)–(B11) of Appendix B. By calculating the real part of G_1, the net gain of phonon is found as

$$\alpha' = \eta_3 - \gamma_m. \quad (31)$$

The definitions of parameters η_i (for $i = 1,2,\ldots,8$) are given in Eqs. (B12)–(B19) of Appendix B.

Realization of phonon lasing requires that the gain α' be a positive value and that the system be in the stable region. From Fig. 3(a), we find that the region with both $\alpha' > 0$ (positive gain condition) and $\mathrm{Re}(\lambda) < 0$ (stability condition) is smaller for $\Delta = g$ than that for $\Delta = g/2$. That is, the region between $|\Omega_1|/(2\pi)$ and $|\Omega_2|/(2\pi)$ is smaller than that between $|\Omega_3|/(2\pi)$ and $|\Omega_4|/(2\pi)$. From Fig. 3(b), we find that the decay rate of the cavity field affects both the stability and the gain. It is seen that smaller decay rate γ_c of the cavity field leads to a larger region for stable phonon lasing; that is, the region between $|\Omega_1|/(2\pi)$ and $|\Omega_4|/(2\pi)$ corresponding to $\gamma_c/(2\pi) = 2.8$ MHz is larger than that between $|\Omega_2|/(2\pi)$ and $|\Omega_3|/(2\pi)$ corresponding to $\gamma_c/(2\pi) = 4.8$ MHz.

With the semiclassical approximation, the phonon field b can be written as a two-dimensional vector $b = (u_1\ u_2)^T$ with $u_1 = \mathrm{Re}(b)$ and $u_2 = \mathrm{Im}(b)$. Thus, we can obtain the dynamical equations for u_1 and u_2 as shown in Eqs. (B20) and (B21) of Appendix B. We should note here that it is usually difficult to define a scalar potential for the mechanical mode.

We now discuss the special case of $\delta = 0$ for which the equations of motion of u_1 and u_2 are given as in Eqs. (B26) and (B27). When $u_1 \gg u_2$, the terms containing u_2 are much smaller than the same order terms including u_1, then we can approximately define a two-dimensional scalar potential

$$V \approx -\eta_1 u_1 - \eta_2 u_2 + \mathrm{Im}(G_1) u_1 u_2 - \frac{\alpha'}{2}\left(u_1^2 + u_2^2\right) - \frac{\varepsilon_6}{3}u_1^3 + \frac{\eta_7}{4}\left(u_1^2 + u_2^2\right)^2 - \eta_8 u_1^3 u_2 - \frac{\eta_8}{3}u_2^3 u_1. \quad (32)$$

The definition of ε_6 is given in Eq. (B22) of Appendix B. Actually, in other parameter regimes, e.g., a larger δ, we may also have $u_2 \gg u_1$, and the scalar potential similar to Eq. (32) can also be obtained.

In Fig. 5, the two-dimensional scalar potential V is plotted as functions of u_1 and u_2. We find that when the coefficients η_1, η_2, and ε_7 are negligibly small, the potential V approximately has a rotating symmetry in the u_1-u_2 plane; otherwise, the symmetry is broken. It is also easily found that the potential V has only one equilibrium point given at $b = (u_1, u_2) = 0$ when $\alpha' < 0$; that is, there is no phonon lasing. We note that it is possible to have nonzero equilibrium points for V if the value of α' is negative but very close to 0. However if $\alpha' > 0$, $b = 0$ is not a stable point. Instead, two new stable points appear in some directions in the u_1-u_2 plane. We find that these two stable points are not symmetric for the nonzero coefficients of odd terms for u_1 and u_2 in Eq. (32) in contrast to the case of the photon lasing [34] in which two stable points are always symmetric. We note that Eq. (30) is valid only near the threshold.

In the case in which the terms including u_2 in V are negligibly smaller than the terms including u_1, then we can neglect all terms including u_2 ($u_1 \gg u_2$) in Eq. (32) and approximately define a one-dimensional scalar potential

$$V \approx -\eta_1 u_1 - \frac{\alpha'}{2}u_1^2 - \frac{\varepsilon_6}{3}u_1^3 + \frac{\eta_7}{4}u_1^4. \quad (33)$$

In Fig. 6, V is plotted as a function of u_1 according to Eq. (33). We also show in Fig. 5 that the shape of the potential function

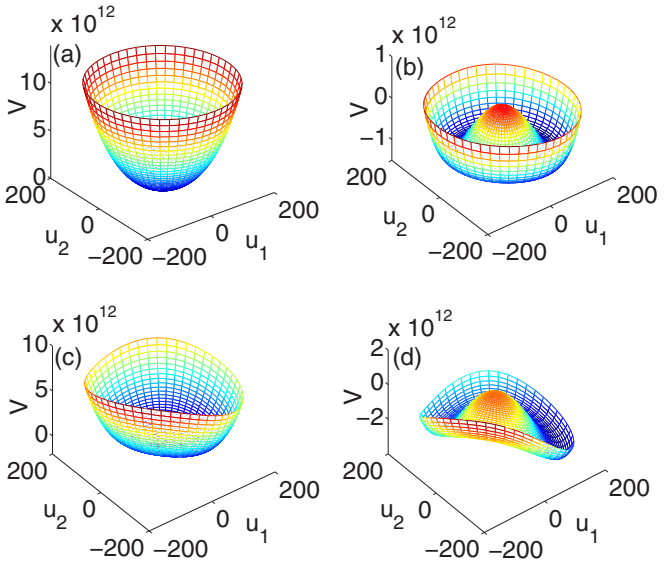

FIG. 5. (Color online) The two-dimensional scalar potential V as functions of u_1 and u_2. The parameters corresponding to the four panels are (a) $\eta_1/(2\pi) = 100$ MHz, $\eta_2/(2\pi) = 50\,\text{MHz}, \alpha'/(2\pi) = -50\,\text{MHz}, \text{Im}(G_1)/(2\pi) = -1\,\text{MHz}, \varepsilon_6/(2\pi) = 2000$ Hz, $\eta_7/(2\pi) = 1800$ Hz, and $\eta_8/(2\pi) = 10$ Hz; (b) $\alpha'/(2\pi) = 36$ MHz, and the other parameters are the same as in (a); (c) $\eta_1/(2\pi) = 1$ GHz, $\eta_2/(2\pi) = 0.5$ GHz, $\alpha'/(2\pi) = -5$ MHz, $\text{Im}(G_1)/(2\pi) = -20$ MHz, $\varepsilon_6/(2\pi) = 0.02$ MHz, $\eta_7/(2\pi) = 2500$ Hz, and $\eta_8/(2\pi) = 100$ Hz; (d) $\alpha'/(2\pi) = 20$ MHz, and the other parameters are the same as in (c).

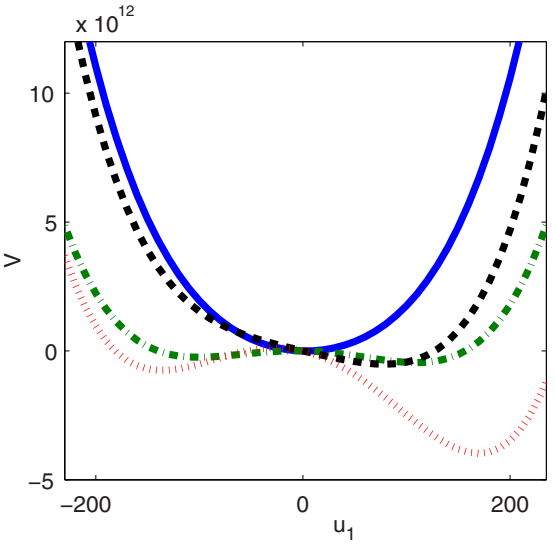

FIG. 6. (Color online) One-dimensional potential V as a function of u_1. The parameters corresponding to four curves are (a) $\eta_1/(2\pi) = 100\,\text{MHz}, \alpha'/(2\pi) = -50\,\text{MHz}, \varepsilon_6/(2\pi) = 2000\,\text{Hz}$, and $\eta_7/(2\pi) = 1800$ Hz (blue solid curve); (b) $\alpha'/(2\pi) = 36$ MHz, the other parameters are the same as in (a) (green dash-dotted curve); (c) $\eta_1/(2\pi) = 1$ GHz, $\alpha'/(2\pi) = -5$ MHz, $\varepsilon_6/(2\pi) = 0.02$ MHz, and $\eta_7/(2\pi) = 2500$ Hz (black dashed curve); (d) $\alpha'/(2\pi) = 20$ MHz, the other parameters are the same as in (c) (red dotted curve).

V changes from the parabolic potential well to two symmetric potential wells, and then to two asymmetric potential wells as the parameters are varied. Actually, a potential similar to that given in Fig. 5 can also be found for u_2 in some parameter regimes.

In summary, we have found that the phonon lasing here is very different from the photon lasing generated by the two-level atomic ensemble. In particular, the phonon lasing might be produced without population inversion in contrast to the photon lasing. This is due to the classical driving to the supermodes. We have also found that the shape of the potential can be changed from the asymmetric to symmetric one with variations of the parameters in the equation of the phonon lasing. However, the potential has only symmetric shape for the equation of the photon lasing.

V. STATISTICAL PROPERTIES OF THE PHONON

We now study the statistical properties of the phonons by calculating the degrees of second-order coherence in the same way as usually done for photons [33]. The normalized equal-time second-order correlation function of the phonons is defined as $g^{(2)}(0) = \langle b^\dagger(t)b^\dagger(t)b(t)b(t)\rangle/\langle b^\dagger(t)b(t)\rangle^2$. Using the small-fluctuation approximation as shown in Eqs. (15)–(17), the degree of second-order coherence can be written as

$$g^{(2)}(0) = \frac{|B_0|^4 + 2\text{Re}\left[B_0^{*2}\langle\beta(t)\beta(t)\rangle\right] + 4|B_0|^2\langle\beta^\dagger(t)\beta(t)\rangle}{[|B_0|^2 + \langle\beta^\dagger(t)\beta(t)\rangle]^2} + \frac{\langle\beta^\dagger(t)\beta^\dagger(t)\beta(t)\beta(t)\rangle}{[|B_0|^2 + \langle\beta^\dagger(t)\beta(t)\rangle]^2}. \quad (34)$$

If the phonon mode is in the coherent state, we have $g^{(2)}(0) = 1$, which corresponds to the phonon lasing.

By introducing the Fourier transform, we can obtain the dynamical equation for the fluctuation operators in the frequency domain as in Eqs. (C4)–(C6) of Appendix C. In this case, we can obtain the phonon fluctuation operators $\beta(t)$ in the frequency domain as follows:

$$\tilde{\beta}(\omega) = p_1(\omega)\tilde{b}_{\text{in}}(\omega) + p_2(\omega)\tilde{b}_{\text{in}}^\dagger(\omega) + p_3(\omega)\tilde{\Gamma}_1(\omega) + p_4(\omega)\tilde{\Gamma}_1^\dagger(\omega) + p_5(\omega)\tilde{\Gamma}_2(\omega) + p_6(\omega)\tilde{\Gamma}_2^\dagger(\omega). \quad (35)$$

The parameters p_i $(i = 1,2,\ldots,6)$ in Eq. (35) are given in Eqs. (C7)–(C12) of Appendix C. From Eqs. (7)–(10), the correlation functions of the input noise operators in the frequency domain can be easily obtained. Then, from Eq. (35), we obtain the correlation functions of the phonon fluctuation operators in the frequency domain as follows:

$$\langle\tilde{\beta}(\omega)\tilde{\beta}(\omega')\rangle = 2\pi\Gamma_{\beta\beta}\delta(\omega+\omega'), \quad (36)$$

$$\langle\tilde{\beta}^\dagger(\omega)\tilde{\beta}(\omega')\rangle = 2\pi\Gamma_{\beta^\dagger\beta}\delta(\omega+\omega'), \quad (37)$$

with the coefficients defined as

$$\Gamma_{\beta\beta}(\omega) = p_1(\omega)p_2(-\omega)(n_b+1) + p_2(\omega)p_1(-\omega)n_b + p_3(\omega)p_4(-\omega)\gamma_c + p_5(\omega)p_6(-\omega)\gamma_c, \quad (38)$$

$$\Gamma_{\beta^\dagger\beta}(\omega) = |p_1(-\omega)|^2 n_b + |p_2(-\omega)|^2(n_b+1) + |p_4(-\omega)|^2\gamma_c + |p_6(-\omega)|^2\gamma_c. \quad (39)$$

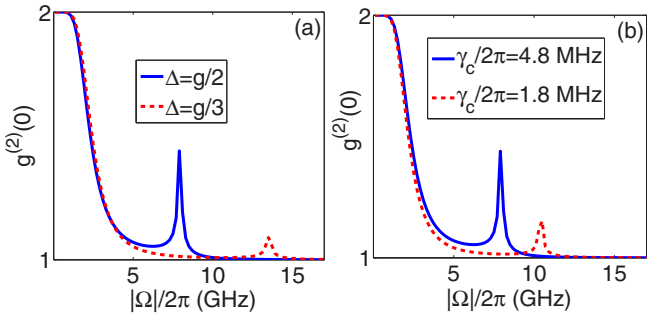

FIG. 7. (Color online) The degree of second-order coherence $g^{(2)}(0)$ as a function of $|\Omega|$. Two curves in (a) correspond to different detunings: $\Delta = g/2$ (blue solid curve) and $\Delta = g/3$ (red dashed curve). However, two curves in (b) correspond to different decay rates of the cavity field: $\gamma_c/(2\pi) = 4.8$ MHz (blue solid curve) and $\gamma_c/(2\pi) = 1.8$ MHz (red dashed curve). The other parameters are the same as in Fig. 2 except $T = 1$ mK.

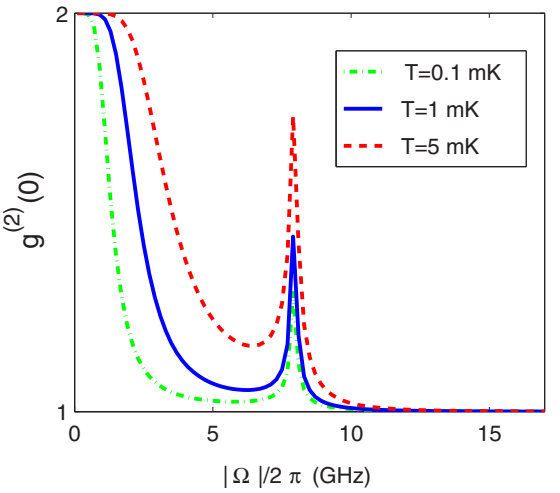

FIG. 8. (Color online) The degree of second-order coherence $g^{(2)}(0)$ as the function of the strength $|\Omega|$ for the driving field. The three curves correspond to different temperatures: (1) $T = 0.1$ mK (green dash-dotted curve); (2) $T = 1$ mK (blue solid curve); (3) $T = 5$ mK (red dash curve). The other parameters are the same as in Fig. 2 except $\Delta = g/2$.

Here, $\Gamma_{\beta\beta}(\omega)$ and $\Gamma_{\beta^\dagger\beta}(\omega)$ represent the correlation spectra of the phonon fluctuation operators. If we assume that the environmental noises have Gaussian distributions, then, from Wick's theorem, all higher-order correlation functions can be written as the combinations of the first- and second-order correlation functions [52]. Thus, with straightforward but tedious calculations, we have $\langle\beta^\dagger(t)\beta^\dagger(t)\beta(t)\beta(t)\rangle = 2Y^2_{\beta^\dagger\beta} + |Y_{\beta\beta}|^2$, where $Y_{\beta\beta}$ and $Y_{\beta^\dagger\beta}$ can be calculated as

$$Y_{\beta\beta} = \langle\beta(t)\beta(t)\rangle = \frac{1}{2\pi}\int_{-\infty}^{+\infty}\Gamma_{\beta\beta}(\omega)d\omega, \tag{40}$$

$$Y_{\beta^\dagger\beta} = \langle\beta^\dagger(t)\beta(t)\rangle = \frac{1}{2\pi}\int_{-\infty}^{+\infty}\Gamma_{\beta^\dagger\beta}(\omega)d\omega. \tag{41}$$

We have calculated the degree of second-order coherence $g^{(2)}(0)$ for the phonons using Eq. (35) to Eq. (41), and plotted it as a function of the coupling strength Ω for different detunings Δ, cavity decay rates γ_c, and temperatures T in Fig. 7(a), Fig. 7(b), and Fig. 8, respectively. All three figures show $g^{(2)}(0) = 2$ when the driving field is not applied to the cavity. This means that the phonons are in the thermal equilibrium state. However, when the coupling strength Ω approaches (or is above) the threshold, the degree of second-order coherence $g^{(2)}(0)$ quickly tends to (or is) unity, which means that the phonon is in a coherent state and the phonon lasing is produced.

In contrast to $g^{(2)}(0) = 1$ with the increase of the intensity of the pumping field in the photon lasing generated by the two-level atomic ensemble [34], we find that there is an additional resonant peak in the curve of $g^{(2)}(0)$ for the phonon lasing when $g^{(2)}(0)$ tends to unity. From Fig. 7(a) and Fig. 7(b), we see that the detuning Δ and the cavity decay rate γ_c affect both the height and the position of the resonant peak. As shown in Fig. 8, the temperature T affects the heights of resonant peaks but has little effect on the positions of the peaks. This means that the properties of the phonon noise are not decoupled from those of the driving optical field. From Eq. (39) we find that the noise spectrum of the phonons in coupled optomechancial system is a function of the coupling strength Ω; this is different from that of the photon lasing generated by two-level atomic ensemble [34]. In fact, the effect of the driving field on the noise spectrum of the optomechanical system has recently been studied [53–56].

To find the relation between the noise spectra of the phonons and $g^{(2)}(0)$, we plot the noise spectra of the phonons in Fig. 9 as functions of the noise frequency ω and the coupling strength $|\Omega|$ using Eq. (39). We note that the parameters in Fig. 9(a) correspond to the noise spectra of the blue-solid curves for $g^{(2)}(0)$ in Fig. 7 and Fig. 8. However the parameters in Fig. 9(b), Fig. 9(c), and Fig. 9(d) correspond to red dashed curves for $g^{(2)}(0)$ in Fig. 7 and Fig. 8, respectively. We find that the positions of the resonant peaks in the phonon noise spectra for Ω are in accordance with those of the degrees of second-order coherence.

Let us now analyze the reasons for the resonant peaks in Fig. 7 and Fig. 8. It is clear from Fig. 9 that there is only one resonant peak for $\Gamma_{\beta^\dagger\beta}$ when Ω is small and fixed but ω is scanned. We also find that the resonant peak is located at proximity of $\omega = -\omega_m$. This coincides well with the result of Eq. (C6). However, with the increase of Ω, we find that several resonant peaks appear and the resonant peak corresponding to $\omega = -\omega_m$ becomes narrower and much higher for given Ω. This results from the Hopf bifurcation phenomena. In fact, the Hopf bifurcation in optomechanical systems has recently been studied [55–57]. In the regime of the Hopf bifurcation, the stabilization of the system is determined by the stable limit cycle [55], and the semiclassical fixed point becomes unstable. If the coupling strength Ω continues to be increased, the Hopf bifurcation disappears finally, and only one resonant peak is left. Both the detuning Δ and the decay rate γ_c affect the position of the critical point of the Hopf bifurcation, whereas the temperature only affects the height of the resonant peak and has little effect on the position of the peak. The existence of a resonant peak will lead to the phonon lasing with low coherence; thus future experiments should avoid the parameter

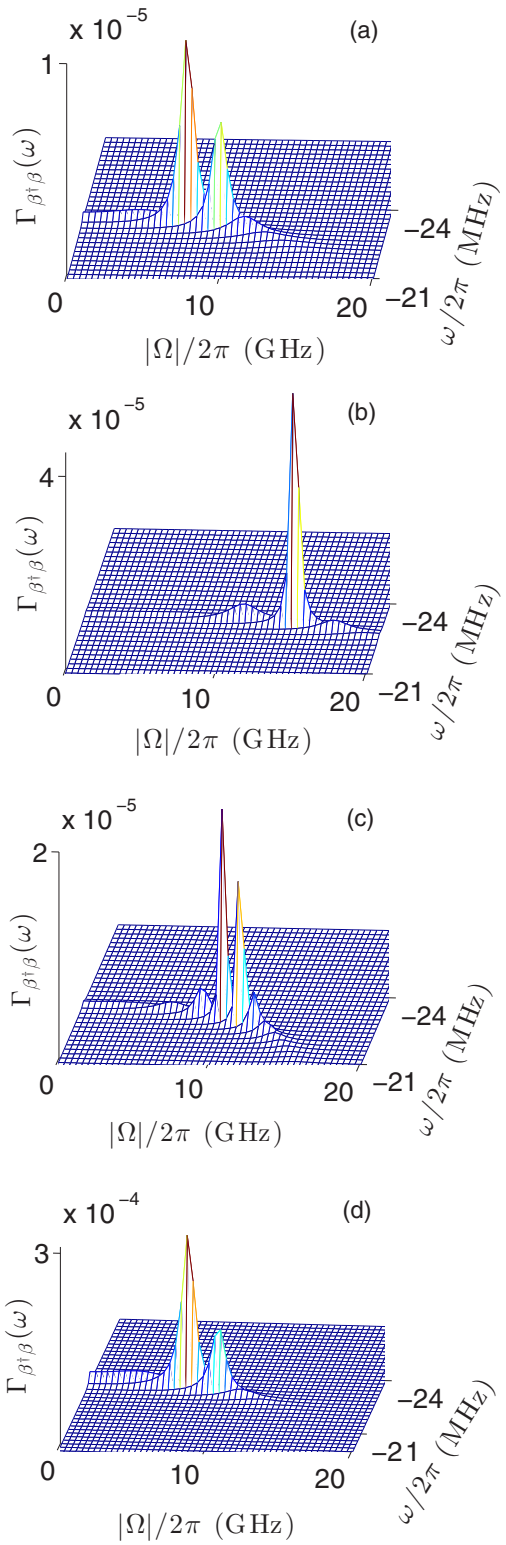

FIG. 9. (Color online) The noise spectrum of phonon $\Gamma_{\beta^\dagger\beta}(\Omega,\omega)$ as the function of the frequency ω and the coupling strength $|\Omega|$. The noise spectrum of blue solid curves for $g^{(2)}(0)$ in Fig. 7(a), Fig. 7(b), and Fig. 8 correspond to (a), while the noise spectra corresponding to red-dashed curves for $g^{(2)}(0)$ in Fig. 7(a), Fig. 7(b), and Fig. 8 are described in (b), (c), and (d), respectively.

values which lead to the appearance of such peaks. In summary, we find that the detuning, cavity decay rate, and temperature significantly affect the coherence of phonon lasing.

VI. CONCLUSIONS

We have theoretically analyzed phonon lasing studied in Ref. [32] for a coupled optomechanical system. We have found that in the steady-state the phonon mode shows unconventional bistability in the regime of the strong driving field. We have derived the equations of the phonon lasing by adiabatically eliminating the cavity modes, and then obtained the gain and threshold of the mechanical amplification. The positive net gain of the phonon lasing can be obtained in a stable regime, and thus it is possible to create stable coherent phonons in a coupled optomechanical system. In particular, we have clarified that the threshold given in Ref. [32] is just a special case for the phonon lasing in coupled optomechanical systems.

Interestingly, our study shows that the phonon lasing generated by photonic supermodes is somewhat different from the photon lasing generated by a two-level atomic system [33]. For example, even when there is no population inversion of the supermodes, the mechanical mode can be amplified. This is because there exist unpaired supermode terms, which are driven by the classical field, in the equation of motion for the phonon lasing. The role of these terms is the same as that of the driven harmonic oscillator, which tends to the coherent state in the steady state. In contrast to the photon lasing generated by the atomic two-level ensemble, the contribution of these driven terms can always be increased by increasing the intensity of the driving field; thus there is no saturation in the phonon lasing studied here. From the phase diagram of the phonon lasing, we have found that a scalar potential can be approximately defined in some special cases. Different from the photon lasing [34], the symmetry of the effective potential for the phonon mode can be broken in some parameter regimes. That is, the potential well can be changed from an asymmetric shape to a symmetric one by tuning the parameters of the system.

We have also studied the statistical properties of the phonon mode via the degree of second-order coherence. We have found that it tends to unity when the driving field is strong enough. This means that the phonon mode can reach a coherent state and the phonon lasing can take place. Moreover, the resonant peaks occur in the degree of second-order coherence when the strength of the driving field satisfies certain conditions. This distinguished difference from the photon lasing [34] is due to the dependence of the phonon fluctuation spectra on the properties of the coupling strength between the cavity field and the classical driving field. In particular, the appearance of the resonant peaks is due to the Hopf bifurcation of the system in the parameter regime of the driving field strength.

In summary, our study has clarified several important points for the phonon lasing in coupled optomechanical systems. We believe that our results will be helpful in designing new experiments and in interpreting their results. They will be of great interest for the efforts to demonstrate the phonon lasing in parity-time (PT) symmetric optical and optomechanical systems [58–60].

ACKNOWLEDGMENTS

This work is partially supported by the National Natural Science Foundation of China under Grant No. 61328502. Y.X.L. is supported by the NSFC under Grant No. 61025022. J.Z. is supported by the NFSC under Grants No. 61174084, No. 61134008, and No. 60904034. Y.X.L. and J.Z. are supported by the National Basic Research Program of China 973 Program under Grant No. 2014CB921401, the Tsinghua University Initiative Scientific Research Program, and the Tsinghua National Laboratory for Information Science and Technology (TNList) Cross-Discipline Foundation. L.Y. and S.K.O. are partially supported by ARO Grant No. W911NF-12-1-0026.

APPENDIX A: DERIVATION OF THE DYNAMICAL EQUATIONS

We consider a coupled optomechanical system consisting of two optical modes and one mechanical mode. The total Hamiltonian including the environmental noises can be written as follows:

$$\begin{aligned} H &= \hbar\omega_c a_L^\dagger a_L + \hbar\omega_c a_R^\dagger a_R + \hbar g(a_L^\dagger a_R + a_R^\dagger a_L) \\ &+ \hbar\omega_m b^\dagger b - \hbar\chi(a_L^\dagger a_L - a_R^\dagger a_R)(b^\dagger + b) \\ &+ i\hbar[\Omega\exp(-i\omega_d t)a_L^\dagger - \text{H.c.}] \\ &+ \hbar\sum_i \omega_{bi} b_i^\dagger b_i + \hbar\sum_i (g_{bi} b b_i^\dagger + \text{H.c.}) \\ &+ \hbar\sum_i \omega_i^{(L)} a_{Li}^\dagger a_{Li} + \hbar\sum_i \left(g_i^{(L)} a_{Li}^\dagger a_L + \text{H.c.}\right) \\ &+ \hbar\sum_i \omega_i^{(R)} a_{Ri}^\dagger a_{Ri} + \hbar\sum_i \left(g_i^{(R)} a_{Ri}^\dagger a_R + \text{H.c.}\right). \end{aligned} \tag{A1}$$

$b^\dagger$ (or b) is the creation (or annihilation) operator of the phonon mode with frequency ω_m. $a_L^\dagger$ (or a_L) and $a_R^\dagger$ (or a_R) represent the creation (or annihilation) operators of the left and right cavity fields, respectively, and the corresponding frequencies of the two bare cavities are both ω_c. χ is the coupling strength between the cavity field and the mechanical resonator, and the interaction strength between the two optical cavities is g. $b_i^\dagger$ (or b_i) is the creation (or annihilation) operator of the ith environmental noise mode coupled with the mechanical resonator with coupling strength g_{bi}. $a_{Li}^\dagger$ (or a_{Li}) and $a_{Ri}^\dagger$ (or a_{Ri}) are the creation (or annihilation) operators of ith environmental noise mode coupled with the optical modes in the left and right cavities with coupling strengths $g_i^{(L)}$ and $g_i^{(R)}$. A classical driving field with frequency ω_d and amplitude Ω is injected into the left cavity. $\Delta = \omega_d - \omega_c$ is the detuning frequency between the diving field and the mode in the left cavity (bare frequency).

We redefine two new optical modes $a_1 = (a_L + a_R)/\sqrt{2}$ and $a_2 = (a_L - a_R)/\sqrt{2}$; then in a rotating reference frame given by the unitary operation

$$U = \exp\left\{-i\omega_d\left[\sum_{i=1}^{2} a_i^\dagger a_i + \sum_i (a_{Li}^\dagger a_{Li} + a_{Ri}^\dagger a_{Ri})\right]t\right\}, \tag{A2}$$

the Hamiltonian can be rewritten as

$$\begin{aligned} H_r &= H_0 + \hbar\sum_i \omega_{bi} b_i^\dagger b_i + \hbar\sum_i (g_{bi} b b_i^\dagger + \text{H.c.}) \\ &+ \hbar\sum_i \omega_i^{(L)} a_{Li}^\dagger a_{Li} + \hbar\sum_i \omega_i^{(R)} a_{Ri}^\dagger a_{Ri} \\ &+ (\hbar/\sqrt{2})\sum_i \left[g_i^{(L)} a_{Li}^\dagger (a_1 + a_2) + \text{H.c.}\right] \\ &+ (\hbar/\sqrt{2})\sum_i \left[g_i^{(R)} a_{Ri}^\dagger (a_1 - a_2) + \text{H.c.}\right], \end{aligned} \tag{A3}$$

with the Hamiltonian H_0 given in Eq. (3). Here we also use the rotating-wave approximation.

With the Hamiltonian in Eq. (A3), we can obtain the Heisenberg-Langevin equations of the total system as follows:

$$\begin{aligned} \dot{a_1} &= -i(g - \Delta)a_1 + i\chi a_2 b + \Omega/\sqrt{2} \\ &- (i/\sqrt{2})\sum_i \left[g_i^{(L)*} a_{Li} + g_i^{(R)*} a_{Ri}\right], \end{aligned} \tag{A4}$$

$$\begin{aligned} \dot{a_2} &= i(g + \Delta)a_2 + i\chi a_1 b^\dagger + \Omega/\sqrt{2} \\ &- (i/\sqrt{2})\sum_i \left[g_i^{(L)*} a_{Li} - g_i^{(R)*} a_{Ri}\right], \end{aligned} \tag{A5}$$

$$\dot{b} = -i\omega_m b + i\chi a_2^\dagger a_1 - i\sum_i g_{bi}^* b_i, \tag{A6}$$

$$\dot{a_{Li}} = -i(\omega_{Li} - \omega_d)a_{Li} - ig_i^{(L)}(a_1 + a_2)/\sqrt{2}, \tag{A7}$$

$$\dot{a_{Ri}} = -i(\omega_{Ri} - \omega_d)a_{Ri} - ig_i^{(R)}(a_1 - a_2)/\sqrt{2}. \tag{A8}$$

Under the Markovian approximation, we introduce the decay rates γ_L, γ_R, and γ_m of the optical modes in the left and right cavities, the mechanical mode as well as the corresponding fluctuation operators [33]; then we can obtain the dynamical equation of the cavity modes and the mechanical modes in Eqs. (4)–(6) by noting that $\gamma_L = \gamma_R = \gamma_c$. The equations of motion of J_-, J_z, and b are obtained in Eqs. (20)–(22). With the condition $\gamma_c \gg \gamma_m$, by eliminating the operator of the cavity modes with adiabatic approximation, we can obtain the equations of motion of the phonon given in Eq. (25), with the corresponding fluctuation operator defined as

$$\begin{aligned} \Gamma(t) &= \alpha[\Gamma_2^\dagger(t)a_1 + a_2^\dagger\Gamma_1(t)] \\ &- \frac{i\alpha\chi}{\sqrt{2}}\left[\frac{\Omega\Gamma_1^\dagger(t)}{N + i\gamma_c\Delta} - \frac{\Omega^*\Gamma_2(t)}{N - i\gamma_c\Delta}\right]b \\ &+ \frac{\alpha\left[\frac{\gamma_c}{2} - i(g - \Delta)\right]\Omega\Gamma_2^\dagger(t)}{\sqrt{2}[N + i\gamma_c\Delta]} + \sqrt{2\gamma_m}b_{\text{in}}(t). \end{aligned} \tag{A9}$$

APPENDIX B: PARAMETERS GIVEN IN SECTION IV C

By adiabatically eliminating the cavity variables, the photon inversion operator J_z can be written as

$$J_z \approx \frac{\Sigma_z(\Delta, \delta)}{(|\varepsilon_1|^2 + 4\chi^2 b^\dagger b)\left(N^2 + \gamma_c^2\Delta^2\right)}, \tag{B1}$$

where the term $\Sigma_z(\Delta,\delta)$ is defined as

$$\begin{aligned}\Sigma_z = {} & g|\Omega|^2\Delta|\varepsilon_1|^2 + 2\chi^2\delta\Delta|\Omega|^2 b^\dagger b \\ & - i\chi|\varepsilon_1|^2|\Omega|^2(b^\dagger N - Nb)/(2\gamma_c) \\ & + \chi|\Omega|^2\{i\varepsilon_1[(N+\Delta^2)/2 + igM/\gamma_c]b + \text{H.c.}\}.\end{aligned} \tag{B2}$$

We have defined $\varepsilon_1 = \gamma_c + i\delta$. In the regime near threshold, $n \ll |\varepsilon_1|^2/(4\chi^2)$, up to the third-order terms J_z can be expanded as follows:

$$J_z = j_0 + j_1 b + j_1^* b^\dagger - j_2 b^\dagger b + j_3 b^\dagger b^\dagger b + j_3^* b^\dagger b b, \tag{B3}$$

with $j_0 = g\Delta|\Omega|^2\varepsilon_3$ and other coefficients j_i (with $i = 1,2,3$),

$$j_1 = i\chi\varepsilon_3|\Omega|^2[M + (\varepsilon_2 M + \gamma_c\varepsilon_1\Delta^2)/|\varepsilon_1|^2]/(2\gamma_c), \tag{B4}$$

$$j_2 = 2\chi^2\Delta\varepsilon_3|\Omega|^2[\omega_m/|\varepsilon_1|^2 + gM\varepsilon_3], \tag{B5}$$

$$\begin{aligned}j_3 = {} & [i\chi^3\varepsilon_3|\Omega|^2/(2\gamma_c|\varepsilon_1|^2)] \\ & \times [(2\varepsilon_3 M^2 - 1)|\varepsilon_1|^2 + 2\varepsilon_3(\varepsilon_2^* M^2 + \gamma_c\varepsilon_1^*\Delta^2 M) \\ & - \varepsilon_2^* + 4M + 4(\varepsilon_2^* M + \gamma_c\varepsilon_1^*\Delta^2)/|\varepsilon_1|^2],\end{aligned} \tag{B6}$$

where the parameters $M = \gamma_c^2/4 + g^2$, $\varepsilon_2 = \gamma_c^2 - 2g\delta + 2ig\gamma_c + i\gamma_c\delta$, and $\varepsilon_3 = 1/(M^2 + \gamma_c^2\Delta^2)$.

Substituting J_z in Eq. (B3) into the dynamical equation of b in Eq. (27), if we define coefficients G_i (for $i = 0,1,\ldots,4$),

$$G_0 = \eta_1 + i\eta_2, \tag{B7}$$

$$G_1 = \eta_3 - \gamma_m - i(\omega_m + \eta_4), \tag{B8}$$

$$G_2 = 2\chi^2 j_1^*/\varepsilon_1 + \eta_5 + i\eta_6, \tag{B9}$$

$$G_3 = 2\chi^2 j_1/\varepsilon_1, \tag{B10}$$

$$G_4 = \eta_7 - i\eta_8, \tag{B11}$$

then the phonon lasing equation near the threshold can be written as in Eq. (30) with the parameters

$$\eta_1 = \chi\gamma_c\varepsilon_3|\Omega|^2(\varepsilon_4 M + 2\delta\Delta^2)/(2|\varepsilon_1|^2), \tag{B12}$$

$$\eta_2 = \chi\varepsilon_3|\Omega|^2\left(\varepsilon_5 M + 2\gamma_c^2\Delta^2\right)/(2|\varepsilon_1|^2), \tag{B13}$$

$$\eta_3 = \gamma_c\chi^2(2j_0 - \delta\Delta|\Omega|^2\varepsilon_3)/|\varepsilon_1|^2, \tag{B14}$$

$$\eta_4 = \chi^2\left(2\delta j_0 + \gamma_c^2\Delta|\Omega|^2\varepsilon_3\right)/|\varepsilon_1|^2, \tag{B15}$$

$$\eta_5 = \gamma_c\chi^3\varepsilon_3|\Omega|^2/(2|\varepsilon_1|^2)[\varepsilon_4 - 2\varepsilon_3 M|\Omega|^2(\varepsilon_4 M + 2\delta\Delta^2)], \tag{B16}$$

$$\eta_6 = \chi^3\varepsilon_3|\Omega|^2/(2|\varepsilon_1|^2)\left[\varepsilon_5 - 2\varepsilon_3 M|\Omega|^2\left(\varepsilon_5 M + 2\gamma_c^2\Delta^2\right)\right], \tag{B17}$$

$$\eta_7 = 2\gamma_c\chi^2\left(j_2 - 2\delta\chi^2\Delta\varepsilon_3^2|\Omega|^2 M\right)/|\varepsilon_1|^2, \tag{B18}$$

$$\eta_8 = 2\chi^2\left(\delta j_2 + \chi^2\gamma_c^2\Delta\varepsilon_3^2|\Omega|^2 M\right)/|\varepsilon_1|^2. \tag{B19}$$

Here we have defined $\varepsilon_4 = \delta + 2g$ and $\varepsilon_5 = \gamma_c^2 - 2\delta g$.

Using the semiclassical approximation, the phonon field b can be written as a two-dimensional vector, $b = (u_1,u_2)^T$. Thus, we can obtain the dynamical equations for u_1 and u_2 as

$$\begin{aligned}\dot{u_1} = {} & \eta_1 + \alpha' u_1 - \text{Im}(G_1)u_2 + (\eta_5 + \varepsilon_6)u_1^2 + \varepsilon_7 u_1 u_2 \\ & + (\eta_5 - \delta\varepsilon_8/\gamma_c)u_2^2 - \left(u_1^2 + u_2^2\right)(\eta_7 u_1 + \eta_8 u_2),\end{aligned} \tag{B20}$$

$$\begin{aligned}\dot{u_2} = {} & \eta_2 + \alpha' u_2 + \text{Im}(G_1)u_1 + (\eta_6 - \varepsilon_8)u_2^2 + \varepsilon_9 u_1 u_2 \\ & + (\eta_6 - \delta\varepsilon_6/\gamma_c)u_1^2 - \left(u_1^2 + u_2^2\right)(\eta_7 u_2 - \eta_8 u_1).\end{aligned} \tag{B21}$$

with the corresponding coefficients

$$\varepsilon_6 = 4\chi^2\gamma_c\text{Re}(j_1)/|\varepsilon_1|^2, \tag{B22}$$

$$\varepsilon_7 = 4\chi^2[\delta\text{Re}(j_1) - \gamma_c\text{Im}(j_1)]/|\varepsilon_1|^2, \tag{B23}$$

$$\varepsilon_8 = 4\chi^2\gamma_c\text{Im}(j_1)/|\varepsilon_1|^2, \tag{B24}$$

$$\varepsilon_9 = 4\chi^2[\gamma_c\text{Re}(j_1) + \delta\text{Im}(j_1)]/|\varepsilon_1|^2. \tag{B25}$$

In the special case of $\delta = 0$, then the conditions $\varepsilon_6 \gg \varepsilon_8,\eta_5,\eta_6$, and also $\eta_7 \gg \eta_8$; the dynamical equations of u_1 and u_2 can be written as

$$\begin{aligned}\dot{u_1} = {} & \eta_1 + \alpha' u_1 - \text{Im}(G_1)u_2 + \varepsilon_6 u_1^2 - \varepsilon_8 u_1 u_2 + \eta_5 u_2^2 \\ & + \eta_8\left(u_1^2 + u_2^2\right)u_1 - \eta_8\left(u_1^2 + u_2^2\right)u_2,\end{aligned} \tag{B26}$$

$$\begin{aligned}\dot{u_2} = {} & \eta_2 + \text{Im}(G_1)u_1 + \alpha' u_2 + \varepsilon_6 u_1 u_2 + (\eta_6 - \varepsilon_8)u_2^2 \\ & + \eta_6 u_1^2 + \eta_8\left(u_1^2 + u_2^2\right)u_2 + \eta_8\left(u_1^2 + u_2^2\right)u_1.\end{aligned} \tag{B27}$$

The conditions $\varepsilon_7 = -\varepsilon_8$ and $\varepsilon_9 = \varepsilon_6$ (for $\delta = 0$) have been used to obtain these equations.

APPENDIX C: DERIVATION OF PHONON FLUCTUATION OPERATOR OF EQUATION (35)

Under the small fluctuation approximation as shown in Eqs. (15)–(17) and from Eqs. (4)–(6), we can write down the dynamical equations for the fluctuation operators as

$$\begin{aligned}\dot{\Lambda}_1(t) = {} & -[\gamma_c/2 + i(g-\Delta)]\Lambda_1(t) + \Gamma_1(t) \\ & + i\chi[A_2\beta(t) + B_0\Lambda_2(t)],\end{aligned} \tag{C1}$$

$$\begin{aligned}\dot{\Lambda}_2(t) = {} & -[\gamma_c/2 - i(g+\Delta)]\Lambda_2(t) + \Gamma_2(t) \\ & + i\chi[A_1\beta^\dagger(t) + B_0^*\Lambda_1(t)],\end{aligned} \tag{C2}$$

$$\begin{aligned}\dot{\beta}(t) = {} & -(\gamma_m + i\omega_m)\beta(t) + \sqrt{2\gamma_m}b_{\text{in}}(t) \\ & + i\chi[A_2^*\Lambda_1(t) + A_1\Lambda_2^\dagger(t)].\end{aligned} \tag{C3}$$

If we introduce the Fourier transform $f(t) = \int_{-\infty}^{+\infty} f(\omega)\exp(-i\omega t)(d\omega/2\pi)$ for arbitrary smooth function $f(t)$, the motion equations for the fluctuation operators in the frequency domain can be written as

$$\begin{aligned}-i\omega\tilde{\Lambda}_1(\omega) = {} & -[\gamma_c/2 + i(g-\Delta)]\tilde{\Lambda}_1(\omega) + \tilde{\Gamma}_1(\omega) \\ & + i\chi[A_2\tilde{\beta}(\omega) + B_0\tilde{\Lambda}_2(\omega)],\end{aligned} \tag{C4}$$

$$\begin{aligned}-i\omega\tilde{\Lambda}_2(\omega) = {} & -[\gamma_c/2 - i(g+\Delta)]\tilde{\Lambda}_2(\omega) + \tilde{\Gamma}_2(\omega) \\ & + i\chi[A_1\tilde{\beta}^\dagger(\omega) + B_0^*\tilde{\Lambda}_1(\omega)],\end{aligned} \tag{C5}$$

$$-i\omega\tilde{\beta}(\omega) = -(\gamma_m + i\omega_m)\tilde{\beta}(\omega) + \sqrt{2\gamma_m}\tilde{b}_{\rm in}(\omega) + i\chi[A_2^*\tilde{\Lambda}_1(\omega) + A_1\tilde{\Lambda}_2^\dagger(\omega)]. \quad \text{(C6)}$$

By eliminating the fluctuation operators $\tilde{\Lambda}_1(\omega)$ and $\tilde{\Lambda}_2(\omega)$, we can obtain the expression of $\tilde{\beta}(\omega)$ in Eq. (35). The corresponding coefficients p_i $(i = 1,2,\ldots,6)$ are given by

$$p_1 = (\sqrt{2\gamma_m}\lambda_1 - \chi^2 A_2^* B_0 n_2)/D_1, \quad \text{(C7)}$$

$$p_2 = i\chi(A_1 n_2^+ \lambda_1 + i\chi A_2^* B_0 n_1 m_2)/D_1, \quad \text{(C8)}$$

$$p_3 = i\chi[A_1 n_3^+ \lambda_1 + A_2^* + i\chi A_2^* B_0(n_4 + n_1 m_3)]/D_1, \quad \text{(C9)}$$

$$p_4 = i\chi[A_1 n_4^+ \lambda_1 + i\chi A_2^* B_0(n_3 + n_1 m_4)]/D_1, \quad \text{(C10)}$$

$$p_5 = i\chi[A_1 n_5^+ \lambda_1 + i\chi A_2^* B_0(n_6 + n_1 m_5)]/D_1, \quad \text{(C11)}$$

$$p_6 = i\chi[A_1 n_6^+ \lambda_1 + i\chi A_2^* B_0(n_5 + n_1 m_6)]/D_1, \quad \text{(C12)}$$

and the corresponding coefficients $\lambda_i(\omega)$ $(i = 1,2,\ldots,4)$, $m_i(\omega)$ $(i = 1,2,\ldots,6)$, and $n_i(\omega)$ $(i = 1,2,\ldots,6)$ are defined as

$$\lambda_1 = \gamma_c/2 + i(g - \Delta) - i\omega, \quad \text{(C13)}$$

$$\lambda_2 = \gamma_c/2 - i(g + \Delta) - i\omega, \quad \text{(C14)}$$

$$\lambda_3 = \gamma_m + i\omega_m - i\omega, \quad \text{(C15)}$$

$$\lambda_4 = \lambda_1\lambda_2 + \chi^2|B_0|^2, \quad \text{(C16)}$$

$$m_1 = i\chi^3 A_1^* A_2 B_0^*(\lambda_4 + \lambda_4^+)/(D_2\lambda_3^+\lambda_4\lambda_4^+), \quad \text{(C17)}$$

$$m_2 = \sqrt{2\gamma_m}/(\lambda_3^+ D_2), \quad \text{(C18)}$$

$$m_3 = \chi^2 A_1^* B_0^*/(\lambda_3^+\lambda_4 D_2), \quad \text{(C19)}$$

$$m_4 = i\chi A_2(\chi^2|B_0|^2 - \lambda_4^+)/(\lambda_1^+\lambda_3^+\lambda_4^+ D_2), \quad \text{(C20)}$$

$$m_5 = -i\chi\lambda_1 A_1^*/(\lambda_3^+\lambda_4 D_2), \quad \text{(C21)}$$

$$m_6 = -\chi^2 A_2 B_0^*/(D_2\lambda_3^+\lambda_4^+), \quad \text{(C22)}$$

$$n_1 = i\chi(A_1\lambda_1 + i\chi B_0^* A_2 m_1^+)/\lambda_4, \quad \text{(C23)}$$

$$n_2 = -\chi^2 B_0^* A_2 m_2^+/\lambda_4, \quad \text{(C24)}$$

$$n_3 = -\chi^2 B_0^* A_2 m_3^+/\lambda_4, \quad \text{(C25)}$$

$$n_4 = i\chi(B_0^* + i\chi B_0^* A_2 m_4^+)/\lambda_4, \quad \text{(C26)}$$

$$n_5 = -\chi^2 B_0^* A_2 m_5^+/\lambda_4, \quad \text{(C27)}$$

$$n_6 = (\lambda_1 - \chi^2 B_0^* A_2 m_6^+)/\lambda_4, \quad \text{(C28)}$$

with

$$D_1 = \lambda_1\lambda_3 - i\chi A_1 n_1^+\lambda_1 + \chi^2 A_2^* B_0 n_1 m_1 + \chi^2|A_2|^2 \quad \text{(C29)}$$

and $D_2 = 1 + \chi^2|A_2|^2/(\lambda_1^+\lambda_3^+) - \chi^2|A_1|^2\lambda_1/(\lambda_3^+\lambda_4) - \chi^4|B_0|^2|A_2|^2/(\lambda_1^+\lambda_3^+\lambda_4^+)$.

[1] D. Leibfried, R. Blatt, C. Monroe, and D. Wineland, Rev. Mod. Phys. **75**, 281 (2003).

[2] N. W. Ashcroft and N. D. Mermin, *Solid State Physics* (Saunders College Publishing, New York, 1976).

[3] M. Poot and H. S. J. van der Zant, Phys. Rep. **511**, 273 (2012).

[4] X. Hu and F. Nori, Phys. Rev. Lett. **76**, 2294 (1996); **79**, 4605 (1997).

[5] W. A. Kütt, W. Albrecht, and H. Kurz, IEEE J. Quantum Electron. **28**, 2434 (1992).

[6] E. B. Tucker, Phys. Rev. Lett. **6**, 547 (1961).

[7] W. E. Bron and W. Grill, Phys. Rev. Lett. **40**, 1459 (1978).

[8] A. J. Kent, R. N. Kini, N. M. Stanton, M. Henini, B. A. Glavin, V. A. Kochelap, and T. L. Linnik, Phys. Rev. Lett. **96**, 215504 (2006).

[9] G. Bahl, M. Tomes, F. Marquardt, and T. Carmon, Nat. Phys. **8**, 203 (2012).

[10] A. D. O'Connell, M. Hofheinz, M. Ansmann, R. C. Bialczak, M. Lenander, E. Lucero, M. Neeley, D. Sank, H. Wang, M. Weides, J. Wenner, J. M. Martinis, and A. N. Cleland, Nature (London) **464**, 697 (2010).

[11] M. D. LaHaye, J. Suh, P. M. Echternach, K. C. Schwab, and M. L. Roukes, Nature (London) **459**, 960 (2009).

[12] T. Rocheleau, T. Ndukum, C. Macklin, J. B. Hertzberg, A. A. Clerk, and K. C. Schwab, Nature (London) **463**, 72 (2010).

[13] I. Mahboob, K. Nishiguchi, H. Okamoto, and H. Yamaguchi, Nat. Phys. **8**, 387 (2012).

[14] T. J. Kippenberg and K. J. Vahala, Science **321**, 1172 (2008).

[15] X. W. Xu, H. Wang, J. Zhang, and Y. X. Liu, Phys. Rev. A **88**, 063819 (2013).

[16] X. W. Xu, Y. J. Zhao, and Y. X. Liu, Phys. Rev. A **88**, 022325 (2013).

[17] J. Q. Liao, H. K. Cheung, and C. K. Law, Phys. Rev. A **85**, 025803 (2012).

[18] J. Q. Liao and F. Nori, Phys. Rev. A **88**, 023853 (2013).

[19] J. Kabuss, A. Carmele, T. Brandes, and A. Knorr, Phys. Rev. Lett. **109**, 054301 (2012).

[20] J. Kabuss, A. Carmele, and A. Knorr, Phys. Rev. B **88**, 064305 (2013).

[21] A. Khaetskii, V. N. Golovach, X. Hu, and I. Zutic, Phys. Rev. Lett. **111**, 186601 (2013).

[22] J. T. Mendonca, H. Tercas, G. Brodin, and M. Marklund, Europhys. Lett. **91**, 33001 (2010).

[23] E. M. Chudnovsky and D. A. Garanin, Phys. Rev. Lett. **93**, 257205 (2004).

[24] P. A. Fokker, J. I. Dijkhuis, and H. W. de Wijn, Phys. Rev. B **55**, 2925 (1997).

[25] I. Camps and S. S. Makler, Solid State Commun. **116**, 191 (2000).

[26] I. Bargatin and M. L. Roukes, Phys. Rev. Lett. **91**, 138302 (2003).

[27] K. Vahala, M. Hermann, S. Knünz, V. Batteiger, G. Saathoff, T. W. Hänsch, and T. Udem, Nat. Phys. **5**, 682 (2009).

[28] I. Mahboob, K. Nishiguchi, A. Fujiwara, and H. Yamaguchi, Phys. Rev. Lett. **110**, 127202 (2013).

[29] R. P. Beardsley, A. V. Akimov, M. Henini, and A. J. Kent, Phys. Rev. Lett. **104**, 085501 (2010).

[30] J. B. Khurgin, M. W. Pruessner, T. H. Stievater, and W. S. Rabinovich, Phys. Rev. Lett. **108**, 223904 (2012).

[31] J. B. Khurgin, M. W. Pruessner, T. H. Stievater, and W. S. Rabinovich, New J. Phys. **14**, 105022 (2012).
[32] I. S. Grudinin, H. Lee, O. Painter, and K. J. Vahala, Phys. Rev. Lett. **104**, 083901 (2010).
[33] M. O. Scully and M. S. Zubairy, *Quantum Optics* (Cambridge University Press, Cambridge, 1997).
[34] H. Haken, *Light, Vol. II, Laser Light Dynamics* (North-Holland Physics Publishing, Amsterdam, 1985).
[35] Z. R. Gong, H. Ian, Y. X. Liu, C. P. Sun, and F. Nori, Phys. Rev. A **80**, 065801 (2009).
[36] H. Miao, S. Danilishin, T. Corbitt, and Y. Chen, Phys. Rev. Lett. **103**, 100402 (2009).
[37] S. Basiri-Esfahani, U. Akram, and G. J. Milburn, New J. Phys. **14**, 085017 (2012).
[38] G. Heinrich and F. Marquardt, Europhys. Lett. **93**, 18003 (2011).
[39] M. Ludwig, A. H. Safavi-Naeini, O. Painter, and F. Marquardt, Phys. Rev. Lett. **109**, 063601 (2012).
[40] P. Kómár, S. D. Bennett, K. Stannigel, S. J. M. Habraken, P. Rabl, P. Zoller, and M. D. Lukin, Phys. Rev. A **87**, 013839 (2013).
[41] X. W. Xu and Y. J. Li, J. Phys. B **46**, 035502 (2013).
[42] F. Massel, S. U. Cho, J. M. Pirkkalainen, P. J. Hakonen, T. T. Heikkilä, and M. A. Sillanpää, Nat. Commun. **3**, 987 (2012).
[43] M. Zhang, G. S. Wiederhecker, S. Manipatruni, A. Barnard, P. McEuen, and M. Lipson, Phys. Rev. Lett. **109**, 233906 (2012).
[44] C. A. Regal, J. D. Teufel, and K. W. Lehnert, Nat. Phys. **4**, 555 (2008).
[45] J. D. Thompson, B. M. Zwickl, A. M. Jayich, F. Marquardt, S. M. Girvin, and J. G. E. Harris, Nature (London) **452**, 72 (2008).
[46] S. Aldana, C. Bruder, and A. Nunnenkamp, Phys. Rev. A **88**, 043826 (2013).
[47] O. Kyriienko, T. C. H. Liew, and I. A. Shelykh, Phys. Rev. Lett. **112**, 076402 (2014).
[48] F. Elste, S. M. Girvin, and A. A. Clerk, Phys. Rev. Lett. **102**, 207209 (2009).
[49] J. J. Sakurai, *Modern Quantum Mechanics* (Addison Wesley Publishing, New York, 1994).
[50] N. Lörch, J. Qian, A. Clerk, F. Marquardt, and K. Hammerer, Phys. Rev. X **4**, 011015 (2014).
[51] M. Poot, K. Y. Fong, M. Bagheri, W. H. P. Pernice, and H. X. Tang, Phys. Rev. A **86**, 053826 (2012).
[52] K. Børkje, A. Nunnenkamp, and S. M. Girvin, Phys. Rev. Lett. **107**, 123601 (2011).
[53] G. A. Phelps and P. Meystre, Phys. Rev. A **83**, 063838 (2011).
[54] A. H. Safavi-Naeini, J. Chan, J. T. Hill, S. Gröblacher, H. Miao, Y. Chen, M. Aspelmeyer, and O. Painter, New J. Phys. **15**, 035007 (2013).
[55] C. A. Holmes, C. P. Meaney, and G. J. Milburn, Phys. Rev. E **85**, 066203 (2012).
[56] C. A. Holmes and G. J. Milburn, Fortschr. Phys. **57**, 1052 (2009).
[57] G. Heinrich, M. Ludwig, J. Qian, Björn Kubala, and F. Marquardt, Phys. Rev. Lett. **107**, 043603 (2011).
[58] B. Peng, S. K. Ozdemir, F. Lei, F. Monifi, M. Gianfreda, G. L. Long, S. Fan, F. Nori, C. M. Bender, and L. Yang, Nat. Phys. **10**, 394 (2014).
[59] H. Jing, S. K. Ozdemir, X.-Y. Lü, J. Zhang, L. Yang, and F. Nori, Phys. Rev. Lett. **113**, 053604 (2014).
[60] X.-W. Xu, Y.-X. Liu, C.-P. Sun, and Y. Li, arXiv:1402.7222.